

Article

Iron Oxide-Activated Carbon Composites for Enhanced Microwave-Assisted Pyrolysis of Hardwood

Amine Lataf ¹, Andrew E. Khalil Awad ¹ , Bjorn Joos ^{2,3}, Robert Carleer ¹ , Jan Yperman ¹ , Sonja Schreurs ⁴, Jan D'Haen ² , Ann Cuypers ⁵  and Dries Vandamme ^{1,*} 

¹ Analytical and Circular Chemistry, IMO, CMK, Hasselt University, Agoralaan Building D, 3590 Diepenbeek, Belgium; amine.lataf@uhasselt.be (A.L.)

² Institute for Materials Research and Imec Division Imomec (IMO-IMOMEc), Hasselt University, 3590 Diepenbeek, Belgium

³ EnergyVille, Thor Park 8320, 3600 Genk, Belgium

⁴ NuTec, CMK, Hasselt University, Agoralaan Building H, 3590 Diepenbeek, Belgium

⁵ Environmental Biology, CMK, Hasselt University Agoralaan Building D, 3590 Diepenbeek, Belgium; ann.cuypers@uhasselt.be

* Correspondence: dries.vandamme@uhasselt.be

Abstract: A commercial activated carbon (AC) was modified through iron oxide incorporation to obtain microwave absorbers (MWAs) for microwave-assisted pyrolysis. The influence of iron oxide content (5 and 20 wt% Fe₃O₄) and the modification methods were tested as follows: (1) in situ co-precipitation + washing step with Milli-Q; (2) in situ co-precipitation + washing step with Milli-Q/ethanol; and (3) physical iron oxide blending. The resulting MWAs were evaluated on the microwave-assisted pyrolysis of hardwood in a Milestone Flexiwave microwave reactor. The biochar yield varied from 24 wt% to 89 wt% and was influenced by the modification method rather than the iron oxide addition. The MWAs with physically blended iron oxide resulted in biochar yields comparable to conventional biochar (450 °C). Furthermore, the addition of iron oxide-activated carbon composites during the microwave-assisted pyrolysis caused a significant decrease in the biochar's 16 EPA polycyclic aromatic hydrocarbons, mainly by reducing the amount of pyrene in the biochar.

Keywords: activated carbon; iron oxide; microwave absorbers; microwave-assisted pyrolysis; polycyclic aromatic hydrocarbons



Citation: Lataf, A.; Khalil Awad, A.E.; Joos, B.; Carleer, R.; Yperman, J.; Schreurs, S.; D'Haen, J.; Cuypers, A.; Vandamme, D. Iron Oxide-Activated Carbon Composites for Enhanced Microwave-Assisted Pyrolysis of Hardwood. *Environments* **2024**, *11*, 102. <https://doi.org/10.3390/environments11050102>

Academic Editor: Ali Umud Sen

Received: 17 March 2024

Revised: 3 May 2024

Accepted: 7 May 2024

Published: 15 May 2024



Copyright: © 2024 by the authors. Licensee MDPI, Basel, Switzerland. This article is an open access article distributed under the terms and conditions of the Creative Commons Attribution (CC BY) license (<https://creativecommons.org/licenses/by/4.0/>).

1. Introduction

Agricultural residues represent a wide range of unexploited streams with little or no current application. Globally, these residues are annually accountable for approx. 1 billion tonnes [1]. As such, innovative solutions for these residues hold great potential. Thermochemical processes (gasification, liquefaction and pyrolysis) can convert biomass into valuable end-products [2]. Pyrolysis is the thermochemical decomposition of organic material in an inert atmosphere [2,3]. This process yields three end-products: pyrolysis oil, pyrolysis gas and biochar. Pyrolysis oil and gas can be used as fuel to maintain the pyrolysis conditions, whereas biochar can be used in a wide range of applications, including soil amendment and wastewater treatment [3]. The performance of biochars is affected by their physicochemical properties, influenced by the process parameters (e.g., temperature, residence time, mixing rate, heat transfer, . . .), feedstock origin and heating technology (conventional or microwave-assisted heating) [4–6]. Evidence from previous research has shown that microwave-assisted heating is more energy-efficient than its conventional counterpart [7,8]; heat transfer limitations due to conventional heating are reduced during microwave-assisted heating due to volumetric and selective heating [4]. Nevertheless, there are still some disadvantages compared to conventional pyrolysis. For example, the input

material needs to be microwave active to cause a temperature increase inside the cavity. As most biomass streams are microwave-transparent materials, additional microwave absorbers (MWAs) are added before pyrolysis, resulting in the production of biochar [4,7].

Upon microwave irradiation, incident microwaves can be reflected, transmitted and absorbed or a combination of these three processes [9]. MWAs are materials capable of absorbing and converting microwaves into heating energy due to their high interaction with the dielectric and/or magnetic field because of their complex permittivity and permeability, respectively [9,10]. Microwave heating can be described according to the following equation:

$$P(x, y, z) = \omega \cdot (\mu_0 \cdot \mu''_{\text{eff}} \cdot H_{\text{rms}}^2 + \epsilon_0 \cdot \epsilon''_{\text{eff}} \cdot E_{\text{rms}}^2) \quad (1)$$

where P represents the local power generation (W/m^3), ω ($=2\pi f$) the angular frequency of the incident microwave (rad/s), μ_0 the vacuum magnetic permeability ($=4\pi \times 10^{-7} \text{ H}/\text{m}$), μ''_{eff} the complex effective permeability factor, H_{rms} the local magnetic field strength (A/m), ϵ_0 the permittivity of free space ($=8.854 \times 10^{-12} \text{ F}/\text{m}$), ϵ''_{eff} the effective dielectric loss factor and E_{rms} the local dielectric field strength (V/m).

This equation shows that the power generation by MWAs depends on frequency, the microwave field strength (H_{rms} and E_{rms}) and the MWA properties (μ''_{eff} and ϵ''_{eff}). Although most articles simplify this equation by removing the first part related to magnetic field heating, the effect of the latter cannot be neglected for magnetic materials [9].

A widely used MWA for microwave-assisted pyrolysis (MWP) is activated carbon (AC) [9,11], although there are some studies that also investigated the use of metal-based MWAs (Fe, Fe_3O_4 , NaOH, K_2CO_3 , CaCO_3 , ZnCl_2) [4,9,11–14]. These metal-based MWAs may also act as catalysts for pyrolysis gas cracking. However, the use of metal-based MWAs may involve an additional washing step to obtain the final biochar [12]. The efficiency of each MWA depends on its microwave absorption properties, the MWA-to-biomass ratio, mixing behaviour and reactor dimensions [4].

Little is known about the benefits of combining AC-based and metal-based MWAs in MWP. Furthermore, to the best of our knowledge, the use of magnetic dielectric composite materials for MWP has not been studied before. The superior microwave absorption involving these composite materials has been already highlighted in other studies regarding their use in wireless technology, in situ carbothermal reduction of magnetite and for military purposes [15–17]. An additional benefit of using these materials may be their magnetic separation after MWP, which is currently a huge bottleneck when considering scale-up.

The aim of this study is to synthesise iron oxide-activated carbon composites for enhanced microwave-assisted pyrolysis of hardwood biomass. Therefore, commercial AC was modified via three synthesis routes to obtain iron oxide-activated carbon composites. These iron oxide-activated carbon composites were evaluated to be used as MWAs in the MWP of hardwood biomass to produce biochar. The MWAs were characterised using elemental analysis (EA), inductively coupled plasma optical emission spectroscopy (ICP-OES), scanning electron microscopy with energy dispersive X-ray (SEM-EDX) and X-ray diffraction (XRD) analysis. The resulting biochars were characterised (by elemental analysis, thermogravimetric analysis (TGA) and polycyclic aromatic hydrocarbon (PAH) content), and those characteristics were evaluated against biochar produced by conventional pyrolysis at 450°C .

2. Materials and Methods

2.1. Synthesis of the Microwave Absorbers for the Microwave-Assisted Pyrolysis Experiments

The MWAs were obtained through the modification of commercial AC (WP260, Chemviron). The AC was subjected to in situ co-precipitation (methods A and B) of magnetite (Fe_3O_4) or the physical blending (method C) of the appropriate amount of lab-synthesised Fe_3O_4 in a ball mill (Retsch S1, Haan, Germany). Two Fe_3O_4 contents (5 wt% and 20 wt%) were used in this study, alongside the blanks (0 wt% Fe_3O_4) for each modification method. The three different modification methods are listed in detail in Figure 1.

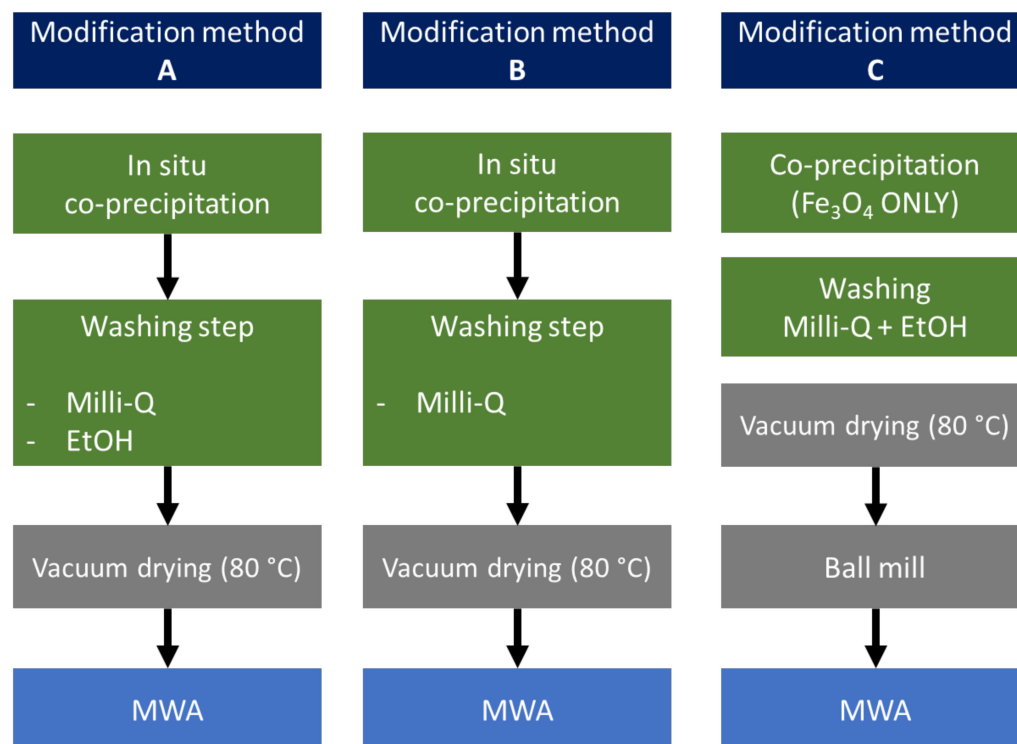
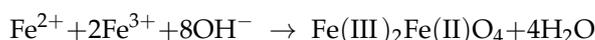


Figure 1. The schematic of the three modification methods used in this study.

The (in situ) co-precipitation method involved the following reaction:



The synthesis of Fe_3O_4 and Fe_3O_4 -loaded AC through the co-precipitation method was adapted from Yazdani et al. [18]. The synthesis of Fe_3O_4 -loaded AC (with a 5 wt% Fe_3O_4 content) involved mixing 25 mL 0.1 M FeCl_2 (EMSURE[®] ACS, Reag. Ph. Eur. for analysis, Supelco[®], Overijse, Belgium) and 50 mL 0.1 M FeCl_3 (EMSURE[®] ACS, Reag. Ph. Eur. for analysis, Supelco[®]) in 300 mL Milli-Q with 10.000 g of AC (1000 mL three-neck round-bottom flask) under a mild N_2 flow. Subsequently, 20 mL of 1M NaOH (EMSURE[®] for analysis, Supelco[®], Overijse, Belgium) was added dropwise (Pumpdrive S001, Heidolph, Schwabach, Germany) under vigorous magnetic stirring. The suspension (pH: 12.7–13.2) was stirred for 12 h before Büchner filtration. After that, the solids were washed and dried in a vacuum oven at 80 °C for 24 h. Depending on the modification method, the washing step was conducted five times using Milli-Q water or a mixture of Milli-Q water and ethanol ($\geq 96.0\%$ (v/v), TechniSolv[®], Leuven, Belgium) (Figure 1). The blanks were obtained using the same procedure as the Fe_3O_4 -loaded MWAs but without the addition of FeCl_2 and FeCl_3 . The blanks' suspension pH was first adjusted with concentrated hydrochloric acid (37%, for Trace Metal Analysis, Primar Plus, Fisher Chemicals, Geel, Belgium) (pH: 2.5–3.1) in order to start at similar conditions as the other experiments.

In order to obtain physically blended Fe_3O_4 -AC MWAs (method C), the appropriate amount of lab-synthesised Fe_3O_4 was added to the AC. The solids were placed in the Retsch S1 ball mill at 70 rpm for 15 min.

Table 1 shows the different MWAs used in this study with their sample codes. The commercial AC WP260 is coded as C0 and contains 0.8 m% Fe. This is considered as a blank for the physically blended samples. The following coding convention was used for the in situ co-precipitation modified MWAs (excluding the blanks): XY with X representing the modification method (A: in situ co-precipitation with Milli-Q and ethanol (EtOH) washing, B: in situ co-precipitation with Milli-Q washing or C: physical blending of Fe_3O_4) and Y representing the expected Fe_3O_4 content (5 or 20 wt%). For the blanks, a slightly different

coding was used because a blank was included at both expected Fe_3O_4 content levels. These blanks were coded as X0-Y, with X representing the modification method (A: in situ co-precipitation with Milli-Q and Ethanol washing, B: in situ co-precipitation with Milli-Q washing or C: physical blending) and Y representing the expected Fe_3O_4 content of the MWA they are associated with.

Table 1. The code of the MWAs according to their modification method and expected Fe_3O_4 content and washing step procedure.

| Microwave Absorber | Modification Method | Washing Step | Expected Fe_3O_4 Content (wt%) |
|--------------------|---------------------|----------------|--|
| A0-5 | A | Milli-Q + EtOH | 0 |
| A0-20 | A | Milli-Q + EtOH | 0 |
| A5 | A | Milli-Q + EtOH | 5 |
| A20 | A | Milli-Q + EtOH | 20 |
| B0-5 | B | Milli-Q | 0 |
| B0-20 | B | Milli-Q | 0 |
| B5 | B | Milli-Q | 5 |
| B20 | B | Milli-Q | 20 |
| C0 | C | Not applicable | 0 |
| C5 | C | Not applicable | 5 |
| C20 | C | Not applicable | 20 |

2.2. Characterisation of the Microwave Absorbers

The MWAs' elemental composition and ash content were measured using the same procedure described by Lataf et al. [19]. The Fe and Na content was measured using ICP-OES analysis (Perkin Elmer Optima 8300, Mechelen, Belgium). This analysis was performed after a two-step microwave digestion (Milestone Ethos, Geel, Belgium) procedure with concentrated nitric acid (HNO_3 , conc; 69 wt% p.a.; Suprapur; Merck, Hoeilaart, Belgium) and hydrogen peroxide (H_2O_2 ; 30 wt% p.a.; Supelco, Merck, Hoeilaart, Belgium). In the first step, 4.0 mL HNO_3 , conc and 6.0 mL H_2O_2 were added to the sample (100 mg) in Teflon vessels. In the second step, 2.0 mL HNO_3 , conc and 1.0 mL H_2O_2 were added to the vessels. The microwave digestion consisted of a heating step (20 °C/min) to 220 °C with a holding time of 15 min. The digested samples were filtered (RotiLab®-round filters, type 14A, Keerbergen, Belgium) and diluted with Milli-Q water to 50.00 mL before analysis. SEM-EDX was conducted on the MWAs at a magnification of $\times 600$ (Phenom Pro X, Thermo Scientific, Geel, Belgium), and, for some MWAs, an additional SEM-EDX was performed on the Zeiss 450 FEGSEM with Gemini 2 optics (Zeiss, Zaventem, Belgium). ImageJ software was used to measure the particle size of the Fe_3O_4 particles [20]. To identify crystalline structures, the MWAs were analysed through XRD (Bruker D8 Discover, Kontich, Belgium) in the 2θ range of 5–65° with a $\text{CuK}\alpha$ radiation source. The crystalline compounds in the MWAs were identified by DIFFRAC.EVA (V6.0) software. The MWAs' specific surface area (S_{BET}) was estimated using the Brunauer-Emmett-Teller (BET) theory with a Rouquerol correction for microporous materials (p/p_0 range: 0.05–0.15). The N_2 adsorption-desorption isotherm was constructed at 77 K using a Tristar II 3020 surface area analyser (Micromeritics, Norcross, GA, USA). The samples (0.5–1 g) were degassed at 150 °C for 16 h under continuous nitrogen flow to remove any residual moisture and volatiles.

2.3. Microwave-Assisted Pyrolysis Experiments

Hardwood (HW) (Biomassaplein, Houthalen, Belgium) was collected and used as a feedstock for MWP). The HW was dried at 105 °C and shredded below 1 cm (Retsch SM100) before the experiment. The HW (18 g) was mixed with 2 g MWA (10 wt% MWA)

and was subjected to MWP (power: 400 W, residence time: 37 min; pressure: 100–600 mbar) in the Milestone FlexiWave (Geel, Belgium) microwave reactor. The reactor temperature was monitored using a grounded type-K thermocouple with a continuous temperature logger (resolution: 2s; EL-GFX-TC, Lascar electronics, Salisbury, UK). Each experiment was performed at least in triplicate and the biochar yield (wt%) was calculated using the following equation:

$$\text{Biochar yield} = \frac{m_{\text{BC}} - m_{\text{MWA}}}{m_{\text{IN}}} \times 100\% \quad (2)$$

where m_{BC} , m_{MWA} and m_{IN} , respectively, represent the mass of the solid fraction after pyrolysis, the mass of the MWA added and the mass of the initial HW/MWA mixture prior to pyrolysis. The resulting biochars were coded as HW-X with X the MWA used during the MWP experiment.

The temperature profile was reported as a mean of the experiments and the maximal temperature T_{max} (°C) was defined as the maximal temperature of the obtained temperature profile. The heating rate δ (°C/min) was calculated by the following equation:

$$\delta = \frac{T_{\text{avg}} - T_0}{\Delta t \times 60} \quad (3)$$

where T_{avg} (°C) is the average temperature during the experiment, T_0 (°C) is the initial temperature of t experiment and Δt (s) is the time until the average temperature T_{avg} is reached.

2.4. Conventional Slow Pyrolysis Experiment

Conventional slow pyrolysis was conducted on HW at 450 °C to compare conventional pyrolysis to the MWP experiments. The experimental setup was a highly modified Nabertherm rotating kiln oven of the type RSRC 120–1000/11 (Lilienthal, Germany) described in detail by Lataf et al. [19] and Haeldermans et al. [21]. The lab-designed modifications included a longer and hollow feeding screw, a chain transmission, a specially designed afterburner, and an insulated discharge to separate the solid material from the gasses. The rotational speed and incline of the rotating kiln were adjusted to have a mean residence time of ± 15 min and was operated at 450 °C. The heated part of the kiln has a length (L) of 1000 mm and an inner diameter (D) of 95 mm. The L/D ratio is therefore 10.5. The inclination angle of the kiln can be adjusted between 0 and 5° and the adjustable rotation of the kiln has a maximum of 40 rpm. The input speed is dependent on the input material, but the adjustable input screw rotates between 0 and 20 rpm. The kiln is unobstructed and without a discharge dam. All experiments were conducted at room temperature (20 °C). The resulting biochar was coded as HW-450.

2.5. Biochar Characterisation

The microwave biochar was sieved at 250 μm to remove the MWA particles (size $< 100 \mu\text{m}$) and ball milled prior to analysis, while the conventional biochar was only ball milled. The elemental composition and ash content were measured similarly to the MWAs (Section 2.2). Proximate thermogravimetric analysis was carried out using the identical procedure described by Vercruyssen et al. [22].

The amount of 16 EPA polycyclic aromatic hydrocarbons (PAHs) in biochar (1 g) was determined according to the International Biochar Initiative (IBI), using US EPA 8270 "Semi volatile Organic Compounds by Gas Chromatography/Mass Spectrometry (GC-MS)" after Soxhlet extraction with 100% toluene (99.5%, AnalaR NORMAPUR®, VWR Chemicals) as extracting solvent [23]. Biochar was passed through a 1 mm sieve and dried at 105 °C prior to a 20 h Soxhlet extraction. The biochar extract was spiked with 1 ppm surrogate standard spiking solution (TraceCERT®, Sigma-Aldrich, Overijse, Belgium) and dried over an anhydrous sodium sulphate column. This purified extract was concentrated to a volume

of 1 mL using a rotary evaporator (70 °C; 100–300 mbar). The total sum of the 16 EPA PAHs ($\sum 16$ PAHs) was calculated according to Equation (4),

$$\sum 16 \text{ PAHs} = \sum C_i \quad (4)$$

where C_i (ppm) is the concentration of the i -th PAHs component.

3. Results and Discussions

3.1. The Microwave-Assisted Pyrolysis Experiments

The MWP experiments with HW were performed to verify the efficiency of the obtained MWAs. The biochar yield (Figure 2) varied from 24 wt% (HW-C20) to 89 wt% (HW-A5). The lowest biochar yields were obtained for HW-C5 (31 wt%) and HW-C20 (24 wt%). These biochars showed the same biochar yield as those obtained from conventional pyrolysis (450 °C; 22 wt%) ($p = 0.38$ (t -test)). The other modification methods (A and B) seemed to result in less microwave-active MWAs, resulting in significantly higher biochar yields (71–89 wt%) compared to HW-C0 (56 wt%) ($p = 5 \times 10^{-14}$). Interestingly, the blanks of modification methods A and B showed a similar behaviour compared to their Fe_3O_4 -loaded MWAs. In contrast, a significant decrease in biochar yield was observed when using physically blended Fe_3O_4 MWAs (C5 and C20) compared to C0. However, increasing the expected Fe_3O_4 content from 5 to 20 wt% did not cause a significant further decrease in the biochar yield ($p = 0.58$).

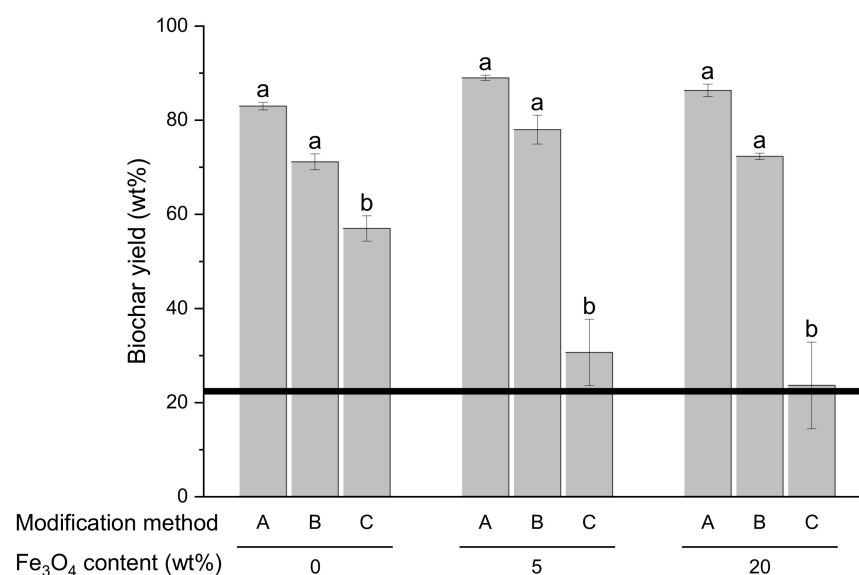


Figure 2. The biochar yield after the MWP experiments (400 W; 10 wt% MWA) with different MWAs ($n = 3$). The solid line represents the HW's biochar yield after conventional pyrolysis (22 wt%; 450 °C). The biochar yields after the MWP with the blanks of modification method A (A0-5 and A0-20) and B (B0-5 and B0-20) are, respectively, represented as A0 and B0. Post-hoc Tukey test (significance level: 0.05). Different letters represent a significant difference in biochar yield.

The higher reactivity of the latter samples was also visible from their temperature profiles (Figure 3). The heating rate during MWP varied between 11 (modification method A) and 32 °C/min (modification method C) and seems independent of the Fe_3O_4 content ($p = 0.81$). The heating rate is mainly controlled by the modification method ($p = 0.02$). The combination of caustic treatment and EtOH washing of the MWAs (modification method A) resulted in a significant decrease in heating rate during MWP compared to the other modification methods ($p = 0.02$). No significant difference was found between the heating rate during MWP with MWAs from modification methods B and C ($p = 0.07$), although there was approx. a 10 °C/min difference in heating rate. During the modification methods A and B, the caustic treatment of the commercial AC (WP260) can facilitate the formation

of chemisorbed oxygen (O), as was also evidenced in previous studies [24,25]. These O-rich sites reduce the initial conjugated π -system responsible for the Maxwell–Wagner polarization mechanisms in ACs [9]. The temperature profiles of the MWP experiments with MWAs from modification methods A and B showed less fluctuations compared to those of modification method C. What is also clear from Figure 3 is that the temperature profiles of modification methods A and B exhibit similar behaviour across all experiments, while the temperature profiles of the experiments with C5 (340 °C) and C20 (384 °C) reached higher temperatures compared to C0 (280 °C) (Table 2). The temperature during MWP might be of great importance, but it cannot completely explain the lower biochar yield achieved when using C0, compared to MWAs from modification method B, although higher temperatures were also reached during these experiments (292–325 °C) (Table 2). However, due to the higher fluctuations measured when using C0, C5 and C20, a possible reason might be the formation of local hotspots that cause extreme local temperature increases in the reactor cavity and can initiate pyrolysis [12]. For this reason, the experiments with the MWAs C0, C5 and C20 had a mean residence time that was approx. ten minutes shorter (27 min) compared to the other experiments (37 min), while still achieving a lower biochar yield.

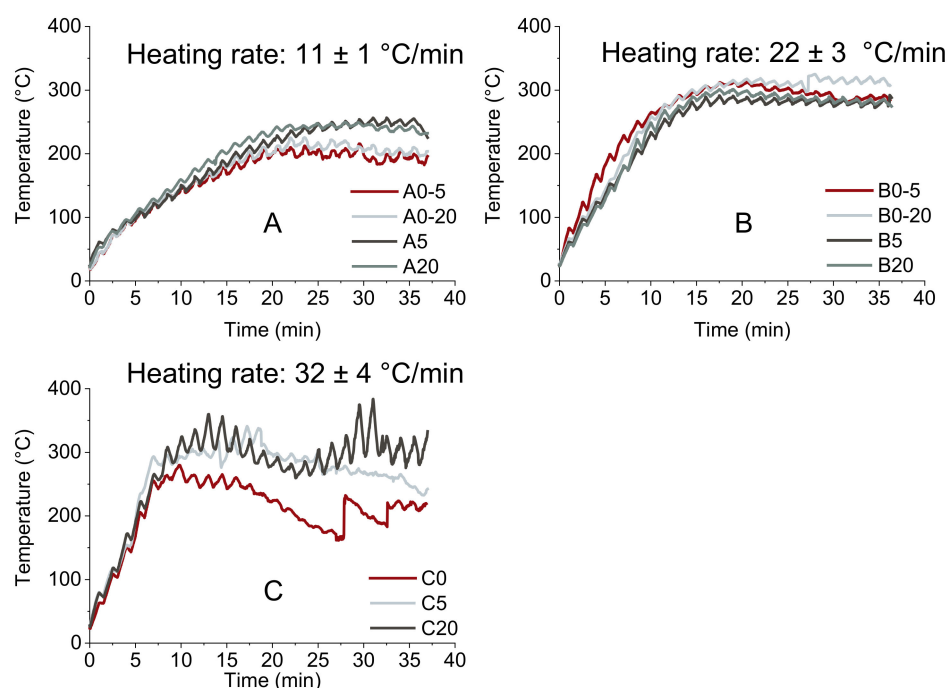


Figure 3. The temperature profile ($n = 3$) of the microwave-assisted pyrolysis experiments divided according to the modification method (A–C) of the MWAs.

Table 2. The mean residence time and maximal temperature of the MWP experiments classified according to the modification method.

| Microwave Absorber | Residence Time (min) | T_{\max} (°C) |
|--------------------|----------------------|-----------------|
| A0-5 | 37 | 216 |
| A0-20 | 37 | 226 |
| A5 | 37 | 257 |
| A20 | 37 | 249 |

Table 2. Cont.

| Microwave Absorber | Residence Time (min) | T _{max} (°C) |
|---------------------------------|----------------------|-----------------------|
| B0-5 | 37 | 313 |
| B0-20 | 34 ± 6 | 325 |
| B5 | 37 | 292 |
| B20 | 37 | 301 |
| C0 | 27 ± 8 | 280 |
| C5 | 27 ± 9 | 340 |
| C20 | 31 ± 6 | 384 |
| Pilot-scale rotary kiln reactor | 14 | 450 |

The higher reactivity of these MWAs is also visible from the higher standard deviation on the biochar yield (between 12–15 wt%). This high reactivity implies that, at a certain point, the pyrolysis experiment could not be controlled anymore due to excessive sparking, which resulted in the earlier shutdown of the experiments. A similar phenomenon was observed by previous studies [26,27]. In order to optimise these experiments, a temperature-controlled cavity instead of a microwave-controlled cavity is recommended. The efficiency of the MWAs can be compared based on the energy requirements to conduct the MWP at a predetermined temperature.

3.2. The Characterisation of the Microwave Absorbers

It is clear from the previous paragraph that the addition of different MWAs caused a difference in the biochar yield and temperature profile during the MWP experiments. In this section, the MWAs are characterised to observe their differences. Furthermore, an explanation for the better performance of the MWAs C5 and C20 was proposed.

Table 3 shows the MWAs' elemental composition and specific surface area. The total carbon (TC) content varied between 62.2 wt% (A20) and 85 wt% (C0). The in situ co-precipitation blanks A0-5/A0-20 and B0-5/B0-20 showed a slightly lower TC (81–82 wt%) content compared to C0 (85 wt%). This decrease in TC was explainable by the increase in O content from 1% up to 6% (B0-5/B0-20). The Fe₃O₄-loaded MWAs A5/A20 showed a higher O content (8.2–9.3 wt%) compared to B5/B20 (4–5 wt%). This suggests that besides the caustic NaOH treatment, the EtOH washing step (of A5/A20) further increased the O content. Previous studies also observed an increase in O content after the caustic treatment of AC with NaOH and demonstrated that this was due to an increase in carboxylic surface functionalities [28,29]. This could partly explain the inferior behaviour of the MWAs from modification methods A and B; the increase in electron-withdrawing oxygen-containing surface functionalities may lead to a disruption in the conjugated π -system responsible for the Maxwell–Wagner polarization [26]. The S_{BET} varied between 920 (C20) and 1190 m²/g (B0-5/B0-20). A slight increase in S_{BET} was observed between C0 (1020 m²/g) and the blanks of modification method A and B (1040–1190 m²/g). A recent study conducted by Hafizuddin et al. also highlighted an increase in S_{BET} after the surface modification with NaOH [29]. The Fe₃O₄-loaded MWAs (940–1130 m²/g) of modification method A and B seemed to have a lower S_{BET}, except for B5 (1130 m²/g).

Figure 4 shows the X-ray diffractogram of C0, A0-5, C5, A5 and A20. The crystalline phases of the blanks (C0 (WP260) and A0-5) consisted of (a) mullite (orthorhombic; Al₄.54Si₁.46O₉.73), (b) quartz (hexagonal; SiO₂) and (d) graphite. The broad peak between 41° and 46° suggests that the ACs also consist of an amorphous carbon phase. In the case of C5 and A20, sharp peaks appeared on the diffractogram corresponding to maghemite (hexagonal; γ -Fe₂O₃). Fe₃O₄ was the targeted compound of the co-precipitation reaction. However, γ -Fe₂O₃ is the oxidation product of Fe₃O₄ ($4\text{Fe}_3\text{O}_4 + \text{O}_2 \rightarrow 6\gamma\text{-Fe}_2\text{O}_3$) [30,31]. The resulting material can therefore be referred to as (superparamagnetic) iron-oxide [30–32].

Strangely, no crystalline iron-rich phases were found in A5, although the SEM-EDX analyses evidenced their presence (Figures S1 and S2 in Supplementary Materials). Further research is necessary to link the magnetic properties to the potential of MWA recovery and to assess the overall recovery ratio and reusability of the recovered MWAs.

Table 3. The total carbon (TC), hydrogen (H), nitrogen (N), oxygen (O) and the specific surface area estimated by the BET theory (S_{BET}) of the MWAs used in this study. Post-hoc Tukey test (significance level: 0.05).

| Microwave Absorber | TC (wt%) | H (wt%) | N (wt%) | O (wt% by diff) | S_{BET} (m ² /g) |
|--------------------|------------|-------------|-------------|-----------------|--------------------------------------|
| C0 | 85 ± 2 | 0.47 ± 0.03 | 0.54 ± 0.08 | 1 ± 2 | 1020 |
| A0-5 | 81 ± 1 | 0.66 ± 0.05 | 0.66 ± 0.04 | 5 ± 1 | 1040 |
| A0-20 | 82 ± 1 | 0.69 ± 0.09 | 0.42 ± 0.04 | 4 ± 2 | 1180 |
| B0-5 | 81.6 ± 0.4 | 0.61 ± 0.06 | 0.51 ± 0.06 | 6.1 ± 0.8 | 1190 |
| B0-20 | 82.0 ± 0.9 | 0.53 ± 0.04 | 0.55 ± 0.07 | 6 ± 1 | 1190 |
| A5 | 72.3 ± 0.6 | 0.50 ± 0.02 | 0.22 ± 0.02 | 9.3 ± 0.9 | 960 |
| A20 | 62.2 ± 0.6 | 0.47 ± 0.02 | 0.21 ± 0.01 | 8.2 ± 0.8 | 940 |
| B5 | 78 ± 1 | 0.7 ± 0.1 | 0.59 ± 0.05 | 4 ± 1 | 1130 |
| B20 | 65.6 ± 0.3 | 0.71 ± 0.07 | 0.48 ± 0.04 | 5.0 ± 0.5 | 980 |
| C5 | 78.8 ± 0.9 | 0.45 ± 0.01 | 0.51 ± 0.05 | 3 ± 1 | 1080 |
| C20 | 69 ± 1 | 0.47 ± 0.01 | 0.57 ± 0.08 | 0 ± 2 | 920 |

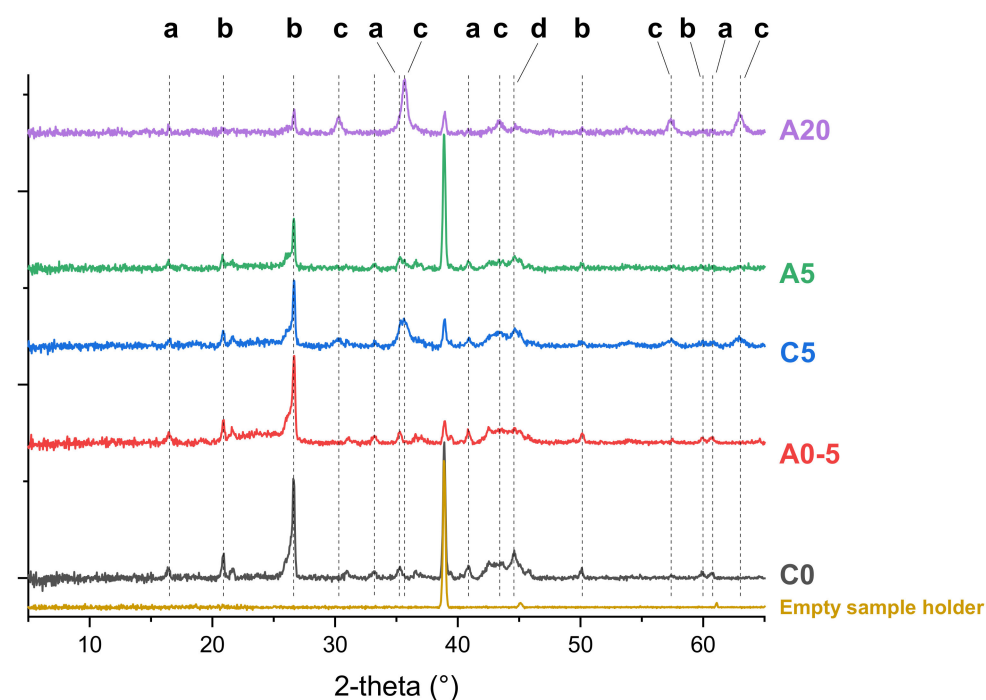


Figure 4. The XRD diffractogram of C0, A0-5, C5, A5 and A20. The letters for each peak represent the corresponding crystal phase: a: mullite ($\text{Al}_{4.54}\text{Si}_{1.46}\text{O}_{9.73}$; orthorhombic); b: quartz (SiO_2 ; hexagonal); c: maghemite ($\gamma\text{-Fe}_2\text{O}_3$; tetragonal); d: graphite C (hexagonal).

To assess the concentration of Fe as Fe_3O_4 , $\gamma\text{-Fe}_2\text{O}_3$ and Na (coming from NaOH) in the MWAs, ICP-OES spectroscopy was used and reported in Table 4. The calculated Fe_3O_4 and $\gamma\text{-Fe}_2\text{O}_3$ content varied, respectively, from 0.81 (B0-5) to 21.5 wt% (C20) and from 0.84 (B0-5) to 22.2 wt% (C20). The calculated Fe_3O_4 content is in the expected range

in the MWAs which further confirms the (in situ) co-precipitation reaction. Additionally, the magnetic behaviour was verified for sample C20, evidencing its potential for magnetic separation (Video S1 in Supplementary Materials). The low residual Na content of the MWAs evidenced that the washing steps successfully washed away the excess Na while retaining the Fe_3O_4 in the MWAs. The ash content increased gradually between 12.3 (A0-5) and 29.8 wt% (C20) with the addition of more Fe_3O_4 (Table 3). MWAs with the same expected Fe_3O_4 content showed a comparable ash content independent of the modification method. However significant differences between them were still observed. The ash content was approx. 10 wt% higher than the Fe content as $\text{Fe}_3\text{O}_4/\gamma\text{-Fe}_2\text{O}_3$ because of the residual minerals such as SiO_2 and mullite (Figure 4) from the C0 (WP260).

Table 4. The iron (Fe) content expressed as Fe_3O_4 and $\gamma\text{-Fe}_2\text{O}_3$, the residual Na content based on ICP-OES spectroscopy and the ash content of the used MWAs.

| Microwave Absorber | Fe as Fe_3O_4 (wt%) | Fe as $\gamma\text{-Fe}_2\text{O}_3$ (wt%) | Na Content (wt%) | Ash (wt%) |
|--------------------|-------------------------------------|--|-------------------|-----------------------|
| C0 | 1.1 * \pm 0.4 | 1.1 \pm 0.4 | 0.06 \pm 0.04 | 13.00 \pm 0.09 e ** |
| A0-5 | 1.23 \pm 0.08 | 1.27 \pm 0.08 | 0.05 \pm 0.02 | 12.33 \pm 0.1 e |
| A0-20 | 1.20 \pm 0.04 | 1.27 \pm 0.08 | 0.12 \pm 0.02 | 12.95 \pm 0.2 e |
| B0-5 | 0.81 \pm 0.01 | 0.84 \pm 0.01 | 0.032 \pm 0.003 | 11.2 \pm 0.3 f |
| B0-20 | 0.82 \pm 0.01 | 0.85 \pm 0.01 | 0.038 \pm 0.002 | 10.8 \pm 0.3 f |
| A5 | 6.14 \pm 0.06 | 6.4 \pm 0.1 | 0.10 \pm 0.01 | 17.7 \pm 0.3 c |
| A20 | 18.3 \pm 0.4 | 18.9 \pm 0.4 | 0.11 \pm 0.03 | 28.9 \pm 0.2 b |
| B5 | 4.25 \pm 0.01 | 4.40 \pm 0.01 | 0.080 \pm 0.001 | 16.5 \pm 0.1 d |
| B20 | 17.7 \pm 0.3 | 18.3 \pm 0.3 | 0.22 \pm 0.01 | 28.2 \pm 0.1 b |
| C5 | 7.2 \pm 0.2 | 7.4 \pm 0.2 | 0.045 \pm 0.001 | 17.6 \pm 0.3 c |
| C20 | 21.5 \pm 0.9 | 22.2 \pm 0.9 | 0.098 \pm 0.001 | 29.8 \pm 0.3 a |

* Fe content expressed as Fe_3O_4 inherently present in untreated commercial AC (WP260). ** Letters (a–f) represent the outcome of an ANOVA analysis ($\alpha = 0.05$). A significant difference in ash content is indicated by a different letter.

The previously discussed data show that there were some compositional differences between the MWAs undergoing the different modifications. This may cause a difference in the microwave absorption behaviour between MWAs of different modification methods. However, the obtained data from the MWP experiments also suggested that the in situ co-precipitation modification showed no advantages over the blanks. In order to explain this behaviour, the morphology and surficial composition of the different MWAs were analysed using SEM-EDX (Figures S1–S3 in Supplementary Materials). A distinct surface was observed when comparing the MWA blanks (A, B, E, F, I) of each modification method with the iron oxide-loaded MWAs (C, D, G, H, K, L). The blanks (method A: A and B; method B: E and F) did not differ much from C0 (I). The in situ co-precipitation method seemed to result in the homogeneous distribution of fine iron oxide nanoparticles. The EDX analysis further evidenced the presence of Fe on the surface (Figure S1). On the other hand, the MWAs modified through physical blending showed a more heterogeneous distribution of larger iron oxide particles on the surface. It is this distribution and the particle size of iron oxide in the MWAs that might hold the critical answer regarding the effectiveness of the MWAs. The small, finely distributed iron oxide particles in the MWAs prepared via in situ co-precipitation behave as microwave-transparent materials because their size is much smaller than the penetration depth of metal oxides such as Fe_3O_4 (approx. 80 μm at 2.45 GHz and 24 °C) [33,34]. Particles that are much smaller than this penetration depth cannot absorb microwaves effectively [33]. The additional change in the surface chemistry due to the alkaline treatment might further explain why MWAs that underwent in situ co-precipitation showed a weak performance during the MWP experiments. On the other

hand, the larger iron oxide particles present in C5 (average size: 28 μm) and C20 (average size: 31 μm) resulted in a higher temperature profile (Figure 3) and a lower biochar yield (Figure 2) compared to C0 (Figure 3), which indicates better thermal degradation. Further research is, however, required to investigate the relative importance of particle distribution and size in relationship to its properties to confirm these findings. The other MWAs did perform worse than the original C0 sample, making them irrelevant for biochar production, as they do not hold great potential when considering scale-up.

3.3. The Characterisation of the Resulting Biochars

In this section, the properties of the resulting biochars were investigated to assess their quality. Only the biochars from the MWP experiments with MWAs C0, C5 and C20 were further investigated. The materials from the other MWAs were irrelevant, as they did not undergo sufficient pyrolysis, as indicated by their high biochar yield (>70 wt%). Table 5 shows the elemental composition (CHNO) and ash content of HW and the obtained biochars. The biochars showed a higher TC content (61–73 wt%), a lower H (3.4–5.3 wt%) and O (18–30 wt%) content and a similar N content (0.5–0.7 wt%) compared to the HW feedstock (TC: 46.7 wt%; H: 5.8 wt%; O: 45 wt%; N: 0.50 wt%). HW-C5 showed a similar composition to HW-450 (TC: 73 wt%; H: 3.11 wt%; O: 18 wt% N:0.57 wt%). There was a decrease in the TC content and an increase in the O content of HW-C20 (TC: 68.5 wt%; O: 23 wt%) compared to HW-C5 (TC:73 wt%; O: 18 wt%). This indicates a higher presence of O-functionalities on the biochar surface, which may have resulted from iron oxide-catalysed oxidation reactions during pyrolysis [35]. As expected, the ash content increased (1.7 (HW)–4.7 wt% (HW-C5)) after MWP due to the decomposition of the HW's organic fraction.

Table 5. The total carbon (TC), hydrogen (H), nitrogen (N), oxygen (O) and ash content of the produced biochars.

| Biochar | TC (wt%) | H (wt%) | N (wt%) | O (wt% by diff) | Ash (wt%) |
|---------|----------------|-----------------|-----------------|-----------------|-----------------|
| HW | 46.7 \pm 0.5 | 5.8 \pm 0.1 | 0.50 \pm 0.05 | 45 \pm 1 | 1.7 \pm 0.2 |
| HW-C0 | 61 \pm 1 | 5.3 \pm 0.2 | 0.7 \pm 0.1 | 30 \pm 1 | 3.21 \pm 0.04 |
| HW-C5 | 73 \pm 2 | 3.9 \pm 0.2 | 0.6 \pm 0.5 | 18 \pm 3 | 4.7 \pm 0.2 |
| HW-C20 | 68.5 \pm 0.7 | 3.4 \pm 0.1 | 0.54 \pm 0.03 | 24.1 \pm 0.9 | 3.5 \pm 0.1 |
| HW-450 | 73 \pm 2 | 3.11 \pm 0.08 | 0.57 \pm 0.03 | 18 \pm 3 | 5.0 \pm 0.6 |

3.4. The Thermal Behaviour of the HW and Its Biochar Samples

Figure 5 shows the thermal behaviour of the HW and the produced biochars between 20 and 600 $^{\circ}\text{C}$. It can be clearly seen from the pyrogram that the thermal stability of the HW increases after pyrolysis. Although HW-C5 and HW-C20 had a similar (C, H and N) composition to HW-450, the thermal stability of the latter was superior to that of the MWP biochars. This could be explained by the lower pyrolysis temperature achieved during the MWP experiments (Figure 3), which caused less degradation of cellulose at peak temperature (360–370 $^{\circ}\text{C}$). In contrast, the shoulder peak around 300 $^{\circ}\text{C}$ (hemicellulose) was not observed anymore for HW-C5 and HW-C20 [36]. This highlights the sequential nature of MWP. Despite the high heating rate during the experiments with C5 and C20, the temperature in the cavity fluctuated around the peak temperature of cellulose (Figure 3), as the heat generated by the MWAs dissipated to its surroundings to volatilise the pyrolysis vapours. The temperature in the cavity will only start to rise after exothermic reactions occur, or the heat generated by the MWAs is higher than the heat of volatilisation of the fractionated volatiles [27].

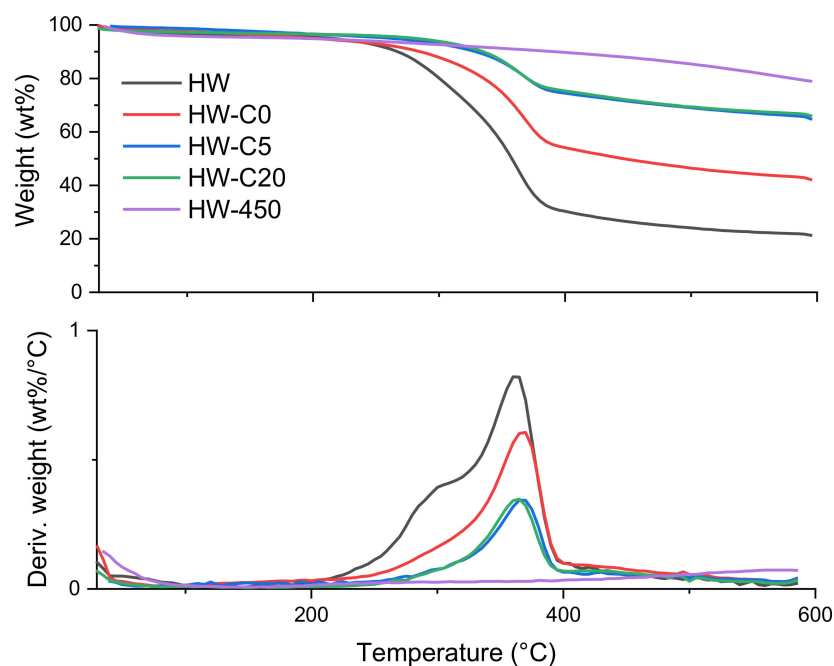


Figure 5. The thermal behaviour (20 °C/min) of HW and the produced biochars under N₂ atmosphere (pyrogram and derivative curve).

3.5. The Biochar PAHs Content

The biochars’ $\Sigma 16$ EPA PAHs content was assessed to evaluate if they can be safely used in applications without causing extensive harm to the environment [37]. This $\Sigma 16$ EPA PAHs content is limited to 6.6 ± 2.2 mg/kg according to EBC guidelines (for agricultural use) [37]. For the selected biochars, the $\Sigma 16$ EPA PAHs content varied between 3.9 mg/kg (HW-C20) and 9.0 mg/kg (HW-450) (Table 6). It seems that MWP decreases the $\Sigma 16$ EPA PAHs content in biochar, as was also evidenced by previous studies on pyrolysis liquids [38,39]. Compared to HW-450, generally, less phenanthrene (PHEN), fluoranthene (FLT), benzo[a]pyrene (B(a)P), indeno(1.2.3-cd)pyrene (IP) and benzo(ghi)perylene (B(ghi)P) were present in the microwave biochars. However, the fluorene (FLU) concentration increased from 0.17 mg/kg (HW-450) up to 1.07 mg/kg (HW-C0).

Table 6. The $\Sigma 16$ EPA PAHs of the produced biochars.

| Biochar | $\Sigma 16$ EPA PAHs (mg/kg) |
|---------|------------------------------|
| HW-450 | 9.0 ± 0.5 |
| HW-C0 | 8.4 ± 0.5 |
| HW-C5 | 6.6 ± 0.9 |
| HW-C20 | 3.9 ± 0.6 |

In this study, it was found that the type of MWA affects the amount of $\Sigma 16$ EPA PAHs, and the expected Fe₃O₄ content is a significant factor in reducing the $\Sigma 16$ EPA PAHs concentration ($p = 0.004$). At first, one would expect this was due to the volatilisation of these semi-volatile compounds because of the increase in temperature during the experiment (Figure 3). However, it seems that the individual PAH constituents behave differently (Figure 6). The highest absolute reduction was observed in HW-C20 for pyrene (PYR) (1.88 mg/kg or 58% decrease), FLU (0.85 mg/kg or 82% decrease) and acenaphthylene (ACY) (0.41 mg/kg or 73% decrease) compared to HW-C0. All other PAHs constituents in HW-C20 decreased by less than 0.1 mg/kg, except for PHEN (0.33 mg/kg or a 54% decrease compared to HW-C0). Naphthalene (NAPH) was the only PAH that showed an increase in

concentration from 0.52 mg/kg (HW-C0) to 1.85 mg/kg (HW-C5). Past research has already highlighted the importance of (biochar-supported) iron oxides in reducing the amount of PAHs in soil, sand and sediment substrates [40,41]. In both studies, a Fe_3O_4 -catalysed Fenton-like oxidation of PAHs involving the formation of free radicals was suggested as a potential mechanism. However, to date, no study has highlighted the occurrence of this phenomenon during MWP.

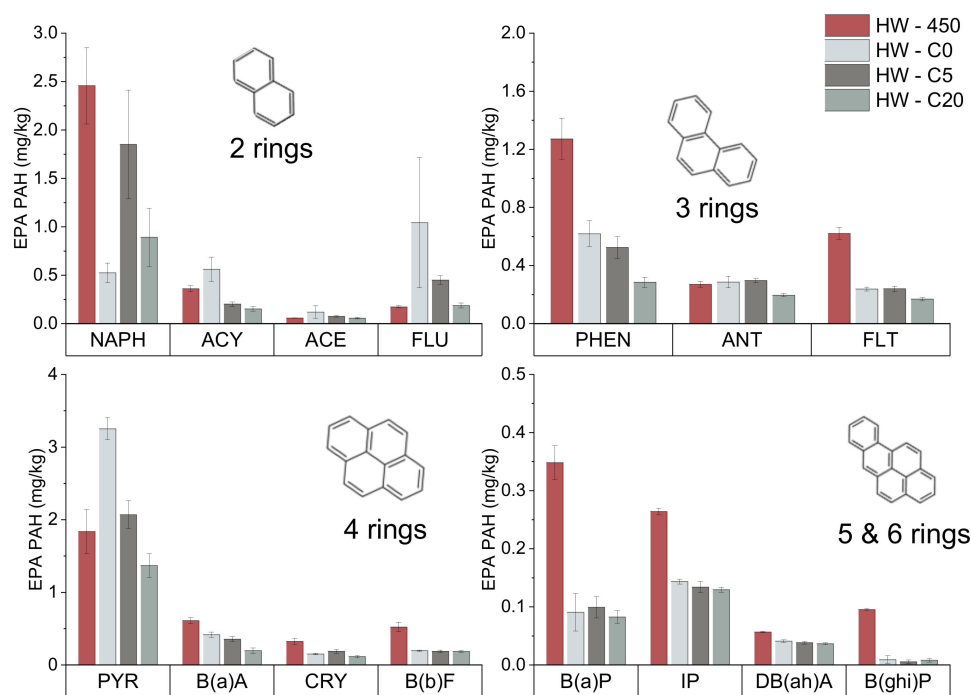


Figure 6. The individual PAHs of the $\Sigma 16$ EPA PAHs for the biochars produced. NAPH: naphthalene, ACY: acenaphthylene, ACE: acenaphthene, FLU: fluorene, PHEN: phenanthrene, ANT: anthracene, FLT: fluoranthene, PYR: pyrene, B(a)A: benzo(a)anthracene, CRY: chrysene, B(b)F: benzo(b)fluoranthene, B(a)P: benzo(a)pyrene, IP: indeno(1,2,3-cd)pyrene, DB(ah)A: dibenz(a,h)anthracene, B(ghi)P: benzo(ghi)perylene.

4. Conclusions

This study shows that the modification method of the AC has a significant effect on pyrolysis, affecting both biochar yield and heating rate. The in situ co-precipitation of iron oxide with commercial AC (WP260) resulted in MWAs with low activity during the MWP experiments, as nano-sized microwave-transparent iron oxide was deposited on the AC surface. AC modification through the ball milling method was the best to obtain MWAs with great potential in MWP. Their resulting biochars (HW-C5 and HW-C20) showed a similar composition to HW-450. Furthermore, a lower $\Sigma 16$ EPA PAHs content can be achieved with an increasing amount of iron oxide in the MWAs.

Supplementary Materials: The following supporting information can be downloaded at: <https://www.mdpi.com/article/10.3390/environments11050102/s1>. Figure S1. The SEM pictures of the different MWAs used. A: A0-5; B: A0-20; C: A5; D: A20; E: B0-5; F: B0-20; G: B5; H: B20; I: C0; J: 100% Fe_3O_4 ; K: C5; L: C20 (Phenom Pro X, Thermo Scientific). Figure S2. The EDX analysis of the different MWAs used. A: A0-5; B: A0-20; C: A5; D: A20; E: B0-5; F: B0-20; G: B5; H: B20; I: C0; J: 100% Fe_3O_4 ; K: C5; L: C20; M: C0 spot analysis; N: C5 spot analysis; O: C20 spot analysis (Phenom Pro X, Thermo Scientific). Figure S3. The SEM pictures of the different MWAs used. A: C0 (10,000 \times); B: C5 (1000 \times); C: A5 (10,000 \times); D: A20 (10,000 \times) (Zeiss 450 FEGSEM with Gemini 2 optics). Video S1. Magnetic AC test-sample C20.

Author Contributions: Conceptualization, A.L., A.C. and D.V.; methodology, B.J., A.L., J.D. and S.S.; validation, R.C., J.Y. and D.V.; formal analysis, A.L.; investigation, A.L. and A.E.K.A.; resources, A.C. and D.V.; data curation, A.L., A.C. and D.V.; writing—original draft preparation, A.L.; writing—review and editing, R.C., J.Y. S.S., A.C. and D.V.; visualization, A.L.; supervision, D.V.; project administration, D.V.; funding acquisition, A.C. and D.V. All authors have read and agreed to the published version of the manuscript.

Funding: This work was financially supported by the Research Foundation Flanders, Belgium (FWO SBO-S000119N).

Data Availability Statement: Dataset available on request from the authors.

Acknowledgments: We would like to acknowledge the technicians who supported and executed some analyses in this study: Elsy Thijssen (ICP-OES), Greet Cuyvers (ICP-OES), Linda Boelenders (GC-MS), Bernard Noppen (GC-MS) and Bart Ruttens (XRD, SEM-EDX).

Conflicts of Interest: The authors declare no conflict of interest.

References

1. Agamuthu, P. Challenges and Opportunities in Agro-Waste Management: An Asian Perspective What Is AgroWaste? 2009. Available online: https://uncrd.un.org/sites/uncrd.un.org/files/inaugural-3r-forum_s2-2-e.pdf (accessed on 5 January 2023).
2. Lee, S.Y.; Sankaran, R.; Chew, K.W.; Tan, C.H.; Krishnamoorthy, R.; Chu, D.-T.; Show, P.-L. Waste to bioenergy: A review on the recent conversion technologies. *BMC Energy* **2019**, *1*, 4. [CrossRef]
3. Oliveira, F.R.; Patel, A.K.; Jaisi, D.P.; Adhikari, S.; Lu, H.; Khanal, S.K. Environmental application of biochar: Current status and perspectives. *Bioresour. Technol.* **2017**, *246*, 110–122. [CrossRef] [PubMed]
4. Li, J.; Dai, J.; Liu, G.; Zhang, H.; Gao, Z.; Fu, J.; He, Y.; Huang, Y. Biochar from microwave pyrolysis of biomass: A review. *Biomass Bioenergy* **2016**, *94*, 228–244. [CrossRef]
5. Mašek, O.; Budarin, V.; Gronnow, M.; Crombie, K.; Brownsort, P.; Fitzpatrick, E.; Hurst, P. Microwave and slow pyrolysis biochar—Comparison of physical and functional properties. *J. Anal. Appl. Pyrolysis* **2013**, *100*, 41–48. [CrossRef]
6. Motasemi, F.; Afzal, M.T.; Salema, A.A.; Mouris, J.; Hutcheon, R.M. Microwave dielectric characterization of switchgrass for bioenergy and biofuel. *Fuel* **2014**, *124*, 151–157. [CrossRef]
7. Haeldermans, T.; Champion, L.; Kuppens, T.; Vanreppelen, K.; Cuypers, A.; Schreurs, S. A comparative techno-economic assessment of biochar production from different residue streams using conventional and microwave pyrolysis. *Bioresour. Technol.* **2020**, *318*, 124083. [CrossRef] [PubMed]
8. Morgan, H.M.; Bu, Q.; Liang, J.; Liu, Y.; Mao, H.; Shi, A.; Lei, H.; Ruan, R. A review of catalytic microwave pyrolysis of lignocellulosic biomass for value-added fuel and chemicals. *Bioresour. Technol.* **2017**, *230*, 112–121. [CrossRef] [PubMed]
9. Sun, J.; Wang, W.; Yue, Q. Review on Microwave-Matter Interaction Fundamentals and Efficient Microwave-Associated Heating Strategies. *Materials* **2016**, *9*, 231. [CrossRef] [PubMed]
10. Muley, P.D.; Boldor, D. Investigation of microwave dielectric properties of biodiesel components. *Bioresour. Technol.* **2013**, *127*, 165–174. [CrossRef]
11. Antunes, E.; Jacob, M.V.; Brodie, G.; Schneider, P.A. Microwave pyrolysis of sewage biosolids: Dielectric properties, microwave susceptor role and its impact on biochar properties. *J. Anal. Appl. Pyrolysis* **2017**, *129*, 93–100. [CrossRef]
12. Haeldermans, T.; Claesen, J.; Maggen, J.; Carleer, R.; Yperman, J.; Adriaenssens, P.; Samyn, P.; Vandamme, D.; Cuypers, A.; Vanreppelen, K.; et al. Microwave assisted and conventional pyrolysis of MDF—Characterization of the produced biochars. *J. Anal. Appl. Pyrolysis* **2019**, *138*, 218–230. [CrossRef]
13. Mohamed, B.A.; Liu, Z.; Bi, X.; Li, L.Y. Co-production of phenolic-rich bio-oil and magnetic biochar for phosphate removal via bauxite-residue-catalysed microwave pyrolysis of switchgrass. *J. Clean. Prod.* **2022**, *333*, 130090. [CrossRef]
14. Undri, A.; Abou-Zaid, M.; Briens, C.; Berruti, F.; Rosi, L.; Bartoli, M.; Frediani, M.; Frediani, P. Bio-oil from pyrolysis of wood pellets using a microwave multimode oven and different microwave absorbers. *Fuel* **2015**, *153*, 464–482. [CrossRef]
15. An, Y.J.; Nishida, K.; Yamamoto, T.; Ueda, S.; Deguchi, T. Microwave absorber properties of magnetic and dielectric composite materials. *Electron. Commun. Jpn.* **2010**, *93*, 18–26. [CrossRef]
16. Ishizaki, K.; Stir, M.; Gozzo, F.; Catala-Civera, J.M.; Vaucher, S.; Nicula, R. Magnetic microwave heating of magnetite–carbon black mixtures. *Mater. Chem. Phys.* **2012**, *134*, 1007–1012. [CrossRef]
17. Wang, L.; Su, S.; Wang, Y. Fe₃O₄–Graphite Composites as a Microwave Absorber with Bimodal Microwave Absorption. *ACS Appl. Nano Mater.* **2022**, *5*, 17565–17575. [CrossRef]
18. Yazdani, F.; Seddigh, M. Magnetite nanoparticles synthesized by co-precipitation method: The effects of various iron anions on specifications. *Mater. Chem. Phys.* **2016**, *184*, 318–323. [CrossRef]
19. Lataf, A.; Jozefczak, M.; Vandecasteele, B.; Viaene, J.; Schreurs, S.; Carleer, R.; Yperman, J.; Marchal, W.; Cuypers, A.; Vandamme, D. The effect of pyrolysis temperature and feedstock on biochar agronomic properties. *J. Anal. Appl. Pyrolysis* **2022**, *168*, 105728. [CrossRef]

20. Schneider, C.A.; Rasband, W.S.; Eliceiri, K.W. NIH Image to ImageJ: 25 years of image analysis. *Nat. Methods* **2012**, *9*, 671–675. [[CrossRef](#)]
21. Haeldermans, T.; Lataf, M.A.; Vanroelen, G.; Samyn, P.; Vandamme, D.; Cuypers, A.; Vanreppelen, K.; Schreurs, S. Numerical prediction of the mean residence time of solid materials in a pilot-scale rotary kiln. *Powder Technol.* **2019**, *354*, 392–401. [[CrossRef](#)]
22. Vercruyse, W.; Smeets, J.; Haeldermans, T.; Joos, B.; Hardy, A.; Samyn, P.; Yperman, J.; Vanreppelen, K.; Carleer, R.; Adriaensens, P.; et al. Biochar from raw and spent common ivy: Impact of preprocessing and pyrolysis temperature on biochar properties. *J. Anal. Appl. Pyrolysis* **2021**, *159*, 105294. [[CrossRef](#)]
23. U.S. EPA. *EPA 8270e: Semivolatile Organic Compounds by Gas Chromatography/Mass Spectrometry*; U.S. EPA: Washington, DC, USA, 2018.
24. Sitthikhankaew, R.; Chadwick, D.; Assabumrungrat, S.; Laosiripojana, N. Performance of sodium-impregnated activated carbons towards low and high temperature H₂S adsorption. *Chem. Eng. Commun.* **2014**, *201*, 257–271. [[CrossRef](#)]
25. Le-Minh, N.; Sivret, E.C.; Shamma, A.; Stuetz, R.M. Factors affecting the adsorption of gaseous environmental odors by activated carbon: A critical review. *Crit. Rev. Environ. Sci. Technol.* **2018**, *48*, 341–375. [[CrossRef](#)]
26. Menéndez, J.A.; Arenillas, A.; Fidalgo, B.; Fernández, Y.; Zubizarreta, L.; Calvo, E.; Bermúdez, J. Microwave heating processes involving carbon materials. *Fuel Process. Technol.* **2010**, *91*, 1–8. [[CrossRef](#)]
27. Wang, X.; Morrison, W.; Du, Z.; Wan, Y.; Lin, X.; Chen, P.; Ruan, R. Biomass temperature profile development and its implications under the microwave-assisted pyrolysis condition. *Appl. Energy* **2012**, *99*, 386–392. [[CrossRef](#)]
28. Chiang, H.-L.; Huang, C.P.; Chiang, P.C. The surface characteristics of activated carbon as affected by ozone and alkaline treatment. *Chemosphere* **2002**, *47*, 257–265. [[CrossRef](#)]
29. Hafizuddin, M.S.; Lee, C.L.; Chin, K.L.; H'ng, P.S.; Khoo, P.S.; Rashid, U. Fabrication of Highly Microporous Structure Activated Carbon via Surface Modification with Sodium Hydroxide. *Polymers* **2021**, *13*, 3954. [[CrossRef](#)]
30. Singh, M.; Ulbrich, P.; Prokopec, V.; Svoboda, P.; Šantavá, E.; Štěpánek, F. Vapour phase approach for iron oxide nanoparticle synthesis from solid precursors. *J. Solid State Chem.* **2013**, *200*, 150–156. [[CrossRef](#)]
31. Li, Z.; Chanéac, C.; Berger, G.; Delaunay, S.; Graff, A.; Lefèvre, G. Mechanism and kinetics of magnetite oxidation under hydrothermal conditions. *RSC Adv.* **2019**, *9*, 33633–33642. [[CrossRef](#)]
32. Borges, R.; Ferreira, L.M.; Rettori, C.; Lourenço, I.M.; Seabra, A.B.; Müller, F.A.; Ferraz, E.P.; Marques, M.M.; Miola, M.; Bairo, F.; et al. Superparamagnetic and highly bioactive SPIONS/bioactive glass nanocomposite and its potential application in magnetic hyperthermia. *Biomater. Adv.* **2022**, *135*, 112655. [[CrossRef](#)]
33. Amini, A.; Ohno, K.; Maeda, T.; Kunitomo, K. Effect of the Ratio of Magnetite Particle Size to Microwave Penetration Depth on Reduction Reaction Behaviour by H₂. *Sci. Rep.* **2018**, *8*, 15023. [[CrossRef](#)] [[PubMed](#)]
34. Hayashi, M.; Yokoyama, Y.; Nagata, K. Effect of Particle Size and Relative Density on Powdery Fe₃O₄ Microwave Heating. *J. Microw. Power Electromagn. Energy* **2010**, *44*, 198–206. [[CrossRef](#)] [[PubMed](#)]
35. Munoz, M.; de Pedro, Z.M.; Casas, J.A.; Rodriguez, J.J. Preparation of magnetite-based catalysts and their application in heterogeneous Fenton oxidation—A review. *Appl. Catal. B Environ.* **2015**, *176–177*, 249–265. [[CrossRef](#)]
36. Díez, D.; Urueña, A.; Piñero, R.; Barrio, A.; Tamminen, T. Determination of Hemicellulose, Cellulose, and Lignin Content in Different Types of Biomasses by Thermogravimetric Analysis and Pseudocomponent Kinetic Model (TGA-PKM Method). *Processes* **2020**, *8*, 1048. [[CrossRef](#)]
37. European Biochar Foundation. *Guidelines for a Sustainable Production of Biochar*; European Biochar Foundation: Arbaz, Switzerland, 2020; pp. 1–22.
38. Ethaib, S.; Omar, R.; Kamal, S.M.M.; Biak, D.R.A.; Zubaidi, S.L. Microwave-Assisted Pyrolysis of Biomass Waste: A Mini Review. *Processes* **2020**, *8*, 1190. [[CrossRef](#)]
39. Dai, Q.; Jiang, X.; Jiang, Y.; Jin, Y.; Wang, F.; Chi, Y.; Yan, J.; Xu, A. Temperature Influence and Distribution in Three Phases of PAHs in Wet Sewage Sludge Pyrolysis Using Conventional and Microwave Heating. *Energy Fuels* **2014**, *28*, 3317–3325. [[CrossRef](#)]
40. Dong, C.-D.; Chen, C.-W.; Kao, C.-M.; Chien, C.-C.; Hung, C.-M. Wood-Biochar-Supported Magnetite Nanoparticles for Remediation of PAH-Contaminated Estuary Sediment. *Catalysts* **2018**, *8*, 73. [[CrossRef](#)]
41. Usman, M.; Faure, P.; Ruby, C.; Hanna, K. Remediation of PAH-contaminated soils by magnetite catalyzed Fenton-like oxidation. *Appl. Catal. B Environ.* **2012**, *117–118*, 10–17. [[CrossRef](#)]

Disclaimer/Publisher's Note: The statements, opinions and data contained in all publications are solely those of the individual author(s) and contributor(s) and not of MDPI and/or the editor(s). MDPI and/or the editor(s) disclaim responsibility for any injury to people or property resulting from any ideas, methods, instructions or products referred to in the content.